

1

Characteristics of safety systems activated by inertial sensors

Saami J. Shaibani

Associate Professor of Physics
Department of Mathematics
Liberty University
Lynchburg, VA 24506

This paper was presented at the 19th Annual Workshop on Human Subjects for Biomechanical Research. It has not been screened for accuracy nor refereed by any body of scientific peers and should not be referenced in the open literature.

Abstract

A crucial element in the successful operation of various safety systems employed in the automotive environment is the performance of the sensors which activate the systems. Inertial sensors are of particular interest because they have seen widespread use in seat belt systems for some time. The more recent advent of inertial sensors in supplemental restraint systems adds to this interest because these systems are becoming increasingly available over a whole spectrum of vehicles. The research performed during this study examines the response of inertial sensors for a range of different impact severities and impact types from laboratory and real-world scenarios. The results show that inertial sensors work well in many cases, but that there are several circumstances in which their action may be delayed or impaired. The effects of such deficiencies are explored by considering the occupant kinematics, and associated injuries, with and without proper deployment of the safety system. Suggestions that may be readily implemented with existing technology are offered for avoiding the problems caused by the inadequate activation of the safety system.

1. Introduction

1.1 Background

The three-point belt^[1-3] was developed for use in passenger vehicles in the 1950s and is perhaps the single most significant safety system ever to be devised. (Superscripted numbers in brackets denote references at the end of the paper.) An important enhancement to the original device was introduced in the 1960s, namely the addition of an emergency locking retractor^[4] (ELR). A

key feature in the ELR is a sensor which, when triggered, activates a locking mechanism which in turn restricts movement in the belt. There are two types of sensor, one that is sensitive to the motion of the vehicle and one that is sensitive to the motion of the belt. The basic nature of the latter involves some sort of flywheel principle, while the former is governed by inertial considerations and is therefore often called an inertial sensor.

The above application of inertial sensors in seat belt systems has now been in place for several decades. Inertial sensors were similarly incorporated into the design of supplemental restraint systems (commonly referred to as "air bags") in the 1960s; however, it has only been more recently that these systems have been installed in passenger vehicles in considerable numbers. The working characteristics of inertial sensors may be determined by empirical means, but this does not always describe their full behavior. The purpose of this research is to explore the fundamental principles that apply to inertial sensors under all types of operating conditions and environments.

1.2 Components in safety systems

Before the specifics of inertial sensors are considered more fully, it may be useful to identify briefly the basic elements of a safety system in which an inertial sensor is just one component. As a rule, a safety system requires a sensor to detect the physical danger that the system is intended to provide protection against. The triggering of the sensor by some precursor to the physical danger is followed by the sensor activating an intermediate mechanism that causes some other component to act against the physical danger. It should be noted that this description is necessarily simplistic and that the number and type of components may vary in different designs. Recent examples of other uses of sensors in automotive safety systems may be found elsewhere^[5].

The terms triggering, activating and actuating tend to be employed synonymously for both the safety system and some of the individual components in the safety system; this is a practice that can introduce some ambiguities but it should not be a problem in this study. In general, there are two basic types of configuration for inertial sensors -- a pendulum striking against some end point near which a locking mechanism is activated, and a ball-and-saucer arrangement in which a ball rolls in a concave saucer until it reaches a point where activation of a mechanical or electrical component occurs. The same principles apply to both types of inertial sensor, but for the sake of illustration the research described in this paper is based on the pendulum device.

2. Methodology and conventions

As established in the previous section, the particular inertial sensor being considered in this research is a pendulum device. A number of assumptions are usually implicit in any treatment of this type of device when its properties are to be determined. It is accepted that the results of such an approach can sometimes be slightly idealized; for example, a pendulum is modeled here as a point mass suspended at the end of an infinitely thin rod, and the point about which the pendulum is pivoted is smooth. These, and similar, first-order approximations are justified because it is generally believed that they do not substantially alter the overall nature of how the device behaves.

A simple exploration of physical principles is undertaken in the context of the geometrical constraints of a particular configuration for the pendulum. The latter can be divided into two general categories -- unidirectional and multidirectional -- which are so different that they are examined separately. Directions of travel for the pendulum are set in accordance with the standard definitions employed for vehicle geometry, namely the positive x direction being forward, the positive y direction being to the right, and the positive z direction being downward. Details of how the rest of the safety system responds after the motion of the pendulum has been derived are beyond the scope of this paper.

3. Inertial sensors in unidirectional insults

3.1 General formulation

Consider a mass m connected to a smooth pivot at the point O via a light inextensible rod. Let the center of mass be at the point P and let the distance OP be ℓ . At time $t = 0$, let P be suspended vertically below O along the positive z direction (Figure 3.01) so that the weight $W = mg$ (where g is the acceleration due to gravity at the surface of the earth) is supported by the tension T in the rod. Now consider the application of an external horizontal load to O in the positive x direction, which is perpendicular to the axis of the pivot. The subsequent motion of O will induce a rotation of the rod about O and this, in turn, will impose a horizontal load on m (Figure 3.02):

$$T \sin\theta = m x''_p \quad (3.01)$$

where θ is the angle of the rod to the vertical and where the subscript P signifies the pendulum. The double prime notation indicates double differentiation with respect to time; likewise, a single prime denotes single differentiation with respect to time.

Figure 3.01

Simple pendulum of mass m and length l with smooth pivot at O

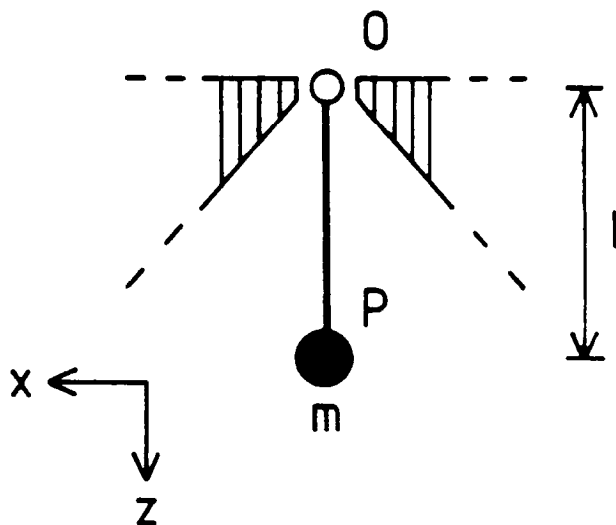


Figure 3.02

Pendulum acceleration x''_p , and forces at pendulum angle θ

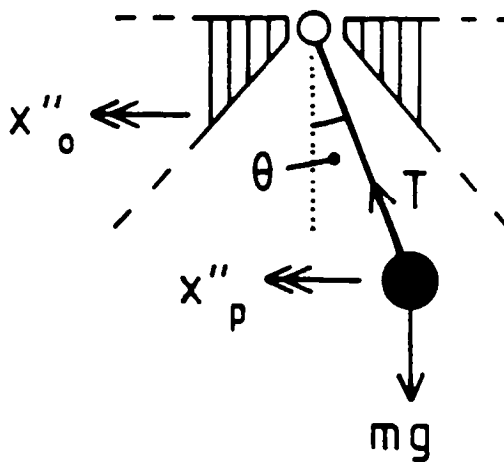
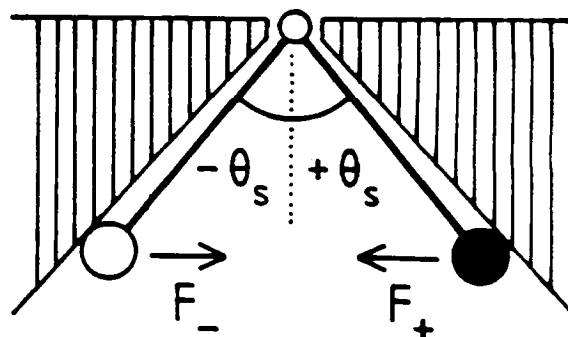


Figure 3.03

Pendulum contact and forces at end points $\theta = +\theta_s$, and $\theta = -\theta_s$



Resolving the motion of P along the line of the rod gives

$$\begin{aligned} T - mg \cos\theta &= \lambda m (v^2/\ell) \\ &= \lambda (m/\ell) \{(x_p - x_0)^2 + (z_p - z_0)^2\} \end{aligned} \quad (3.02a)$$

where $\lambda = (x_0 - x_p) / |x_0 - x_p|$ and the subscript 0 denotes the pivot. The constraint that $(x_p - x_0)^2 + (z_p - z_0)^2 = \ell^2$ means

$$T - mg \cos\theta = f(x_p, x_0, z_0) = 0 \quad (3.02b)$$

The approximation of f as zero is an analytical device only and will be valid if subsequent results are reasonable. Combining equations (3.01) and (3.02b) produces

$$x''_p = g \sin\theta \cos\theta \quad (3.03)$$

$$\text{But,} \quad \sin\theta = (x_0 - x_p) / \ell = f_1(x_0, x_p) \quad (3.04)$$

$$\text{and} \quad \cos\theta = \sqrt{1 - \sin^2\theta} = f_2(x_0, x_p) \quad (3.05)$$

$$\text{Therefore,} \quad x''_p = g f_1 f_2(x_0, x_p) \quad (3.06)$$

Explicit analytical solutions for this second-order differential equation in x_p exist only for certain special x_0 , and in the general case numerical methods must be invoked. The response of the pendulum depends on the motion of the pivot, which is assumed to be the same as that part of the vehicle in which it is located (Figure 3.02). Data for vehicle motion are derived from real-world experimental crash pulses and, for full frontal impacts, these may be fitted to a sinusoidal function of time t

$$x''_0(t) = -a \sin(\pi t/\Delta t) \quad (3.07)$$

where a is the magnitude of the peak deceleration and Δt is the duration of the impact event. Similar behavior can also be expected -- with opposite polarity -- for full rear impacts, but other unidirectional insults may not always be so readily fitted.

It can be shown that

$$a = (\pi \Delta v) / (2 \Delta t) \quad (3.08)$$

where Δv is the change in velocity resulting from equation (3.07). A typical value of Δt in a subcompact vehicle impact might be

$$\Delta t = 100 \text{ milliseconds (msec) [say] (3.09)}$$

for $\Delta v = 48 \text{ kilometers per hour (kph) (3.10)}$
[= 30 miles per hour (mph)]

while compact, intermediate and full-size vehicles might have $\Delta t = 120, 150$ and 200 milliseconds [say], respectively, for the same Δv . The former values give

$$a = 21.5 \text{ g (3.11)}$$

whereas the latter values produce absolute maximum decelerations of $17.9, 14.3$ and 10.7 g , respectively.

A numerical solution for equation (3.06) may now be obtained from an actual measurement of

$$\ell = 1.8 \text{ centimeters (cm) (3.12)}$$

[= 0.7 inches (in)]

in conjunction with suitable values from equations (3.08) to (3.11) and double integration of equation (3.07).

3.2 Contact with the end points

The range of the pendulum motion described in equation (3.06) is physically restricted by the presence of two end points (Figure 3.03), contact with which is usually required for the safety system to be activated. The end points are assumed to be symmetrical about the neutral vertical rest position at $\theta = 0$, and the choice of the symbol S as the subscript for the striking of the pendulum against the end points means that they may be labeled $\theta = \pm \theta_s$. (It is recognized that some designs incorporate an offset in the neutral rest position, and/or a bias in the location of one of the end points, in order to reduce the possibility of inadvertent activations.) The rebound force F at $\theta = \pm \theta_s$ will depend on the extent to which the pendulum tries to go beyond each end point, and a simple estimate for this would be the linear behavior

$$F = k (\theta - \theta_s) \quad \text{for } \theta > + \theta_s \quad [= F_{+VE}] \quad (3.13)$$

$$= 0 \quad \text{for } - \theta_s \leq \theta \leq + \theta_s \quad (3.14)$$

$$= k (\theta + \theta_s) \quad \text{for } \theta < - \theta_s \quad [= F_{-VE}] \quad (3.15)$$

This force will affect the motion of the pendulum and equation (3.06) becomes

$$x''_p = g f_1 f_2(x_0, x_p) + F/m \quad (3.16)$$

As with equation (3.06), explicit analytical solutions for x_p exist only for certain special x_0 and F , and in the general case numerical methods must be invoked. The first term has already been evaluated in the earlier treatment of equation (3.06), and the second term may be determined by empirical measurements taken from a standard pendulum configuration with

$$\theta_s = 20 \text{ degrees} \quad (3.17)$$

and $k/m = 40 \text{ g per degree} \quad (3.18)$

The above values, and those from the previous section, produce an initial pendulum motion with θ negative. The pendulum makes contact with an end point after a time of travel t_s and the first rebound occurs. The extent of this first rebound, and subsequent rebound events, indicate that the energy of the pendulum is not being absorbed during its impacts with the end points. A different approach is presented in the next section to describe pendulum motion beyond t_s in more detail.

3.3 Energy absorption at the end points

The velocity of the pendulum may be considered relative to that of the end points, which share the same kinematics as the pivot because they are both connected to the vehicle (Figure 3.02). Thus,

$$x'_p = x'_o + (x'_p - x'_o) \quad (3.19)$$

When the pendulum strikes the end points $\theta = \pm \theta_s$, any subsequent rebound affects only the relative velocity component

$$x'_p = x'_o + c (x'_p - x'_o) \quad (3.20)$$

where c is the coefficient of restitution with values of

$$c = -1 \quad \text{for elastic rebound} \quad (3.21)$$

$$-1 < c < 0 \quad \text{for inelastic rebound} \quad (3.22)$$

$$c = 0 \quad \text{for zero rebound} \quad (3.23)$$

(Mathematically, c may be set to $+1$ for the free flight of the pendulum before the first rebound and between subsequent rebound events.) The constraint that the range of c is finite suggests an exponential formula

$$c = -\exp \{ -b | \theta - \theta_s | \} \quad (3.24)$$

where b is some absorption coefficient whose value may be matched to experimental results. The dependence of c on θ means that c can also be expressed in terms of x_o and x_p (cf. equations (3.04) and (3.05)), so that

$$c = f_3(x_o, x_p) \quad (3.25)$$

This allows equation (3.20) to be rewritten

$$x'_p = f_4(x_o, x_p) \quad (3.26)$$

The pendulum response governed by equations (3.06) and (3.26) may be calculated numerically, and the results are given in Figure 3.04 for an arbitrary initial value of $b = 0.1$. The figure shows that the first rebound occurs at $\theta = -\theta_s$ after a travel time t_s of 18 milliseconds. The subsequent motion contains a series of local maxima in the pendulum angle θ between successive rebounds at that same end point. The envelope of the maxima is roughly sinusoidal, possibly reflecting the form of the deceleration pulse which is also included in the figure. The average time between each rebound is about 13 milliseconds, which is different from the natural period τ of the pendulum

$$\begin{aligned} \tau &= 2 \pi \sqrt{\ell/g} \\ &= 269 \text{ milliseconds} \end{aligned} \quad (3.27)$$

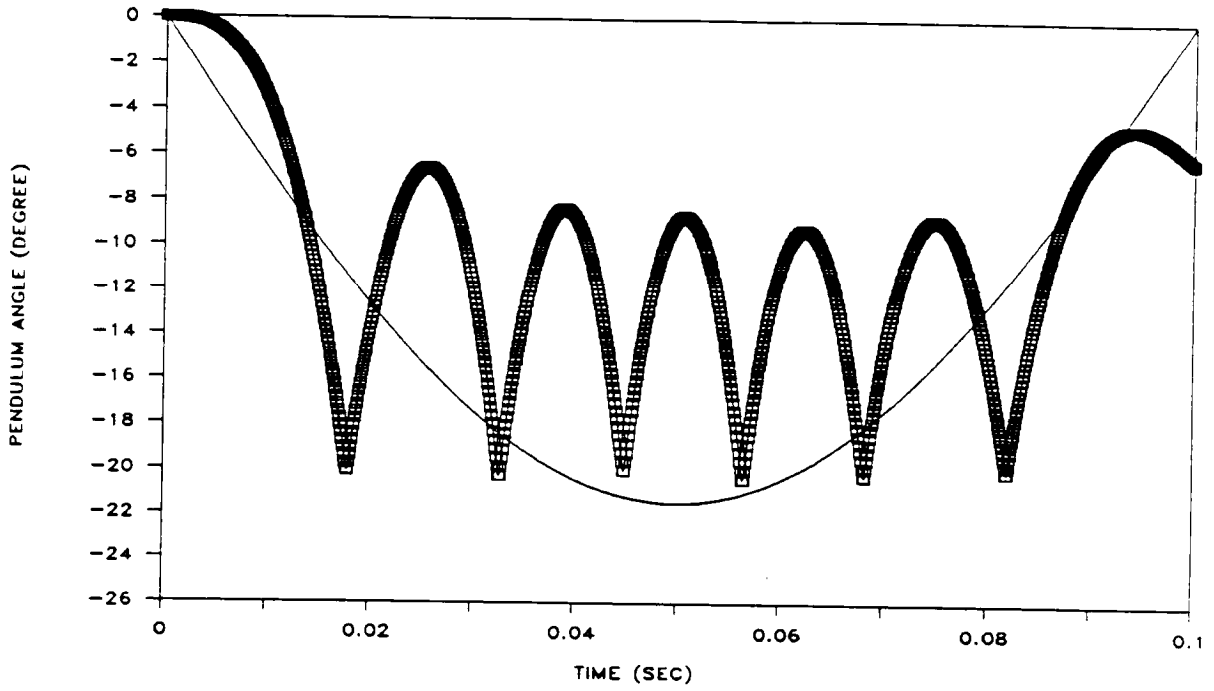


Figure 3.04 Motion of pendulum (symbols) for half sine pulse (line, in g) of $\Delta v = 48$ kph [30 mph] when $b = 0.1$

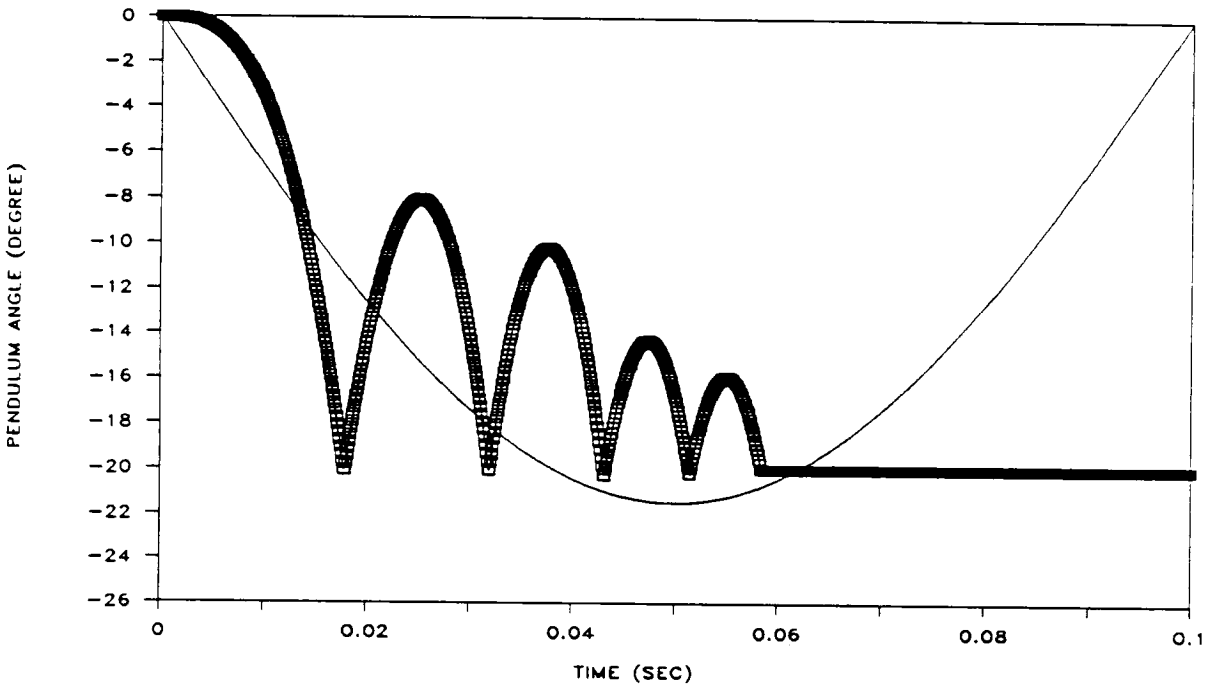


Figure 3.05 Motion of pendulum (symbols) for half sine pulse (line, in g) of $\Delta v = 48$ kph [30 mph] when $b = 1$

The height of the final local maximum in Figure 3.04 indicates some attenuation in the motion of the pendulum due to absorption at the end point. The nature of this absorption may be investigated further by considering different values of the absorption coefficient b . When b is increased by one order of magnitude, the motion of the pendulum until $t = t_s$ is the same as in Figure 3.04 but it then comes to rest against the end point $\theta = -\theta_s$ after striking it five times (Figure 3.05).

The effect of other values of b is demonstrated in Figures 3.06 through 3.09, all of which show the same behavior until $t = t_s$ and then vary in the number of strikes n_s against the end point before coming to rest against the end point. A summary of how n_s depends on b in Figures 3.05 through 3.09 is given in Table 3.1. The values of b in the table are necessarily approximate because the same n_s can arise from more than one value in a range of b , the precise delineation of which would require extensive effort.

The most appropriate value of b may be determined by matching n_s with experimental tests, which should also indicate how well the pendulum acts as the trigger component in the safety system when it strikes the end point. The effectiveness of the pendulum contact with the end point may be affected by the force with which the pendulum strikes the end point and by the time that it spends there. If either of these is inadequate, activation of the safety system could be delayed until a subsequent contact of sufficient strength and duration has been made. The response of the other components in the safety system after it has been triggered by the pendulum will then determine the overall performance of the system.

The travel time t_s of 18 milliseconds to reach the first end point in Figures 3.04 to 3.09 is compared in Table 3.2 with the travel times for other values of Δv and Δt . All the values in the table appear to provide quick enough activation of the safety system if triggering by the pendulum is successful at the first contact.

3.4 Comparison between real-world and laboratory insults

Two real-world crash pulses taken from nearly full frontal impacts of full-size vehicles are displayed in Figures 3.10 and 3.11, and they may be labeled R1 and R2 for convenience. Also included in the figures are the corresponding laboratory equivalents, here called L1 and L2, which are defined by half sine wave pulses with the same Δv and Δt as R1 and R2. The graphical information in the figures may be complemented by characterizing the four pulses in terms of the parameters in Table 3.3, where a_{MAX} is the maximum absolute acceleration and $v_{i=0}$ is the initial velocity. The latter is set to be the same as Δv in the two laboratory pulses L1 and L2.

The effect of R1 and L1 on the motion of the pendulum is plotted in Figures 3.12 and 3.13, which reveal some differences in the travel

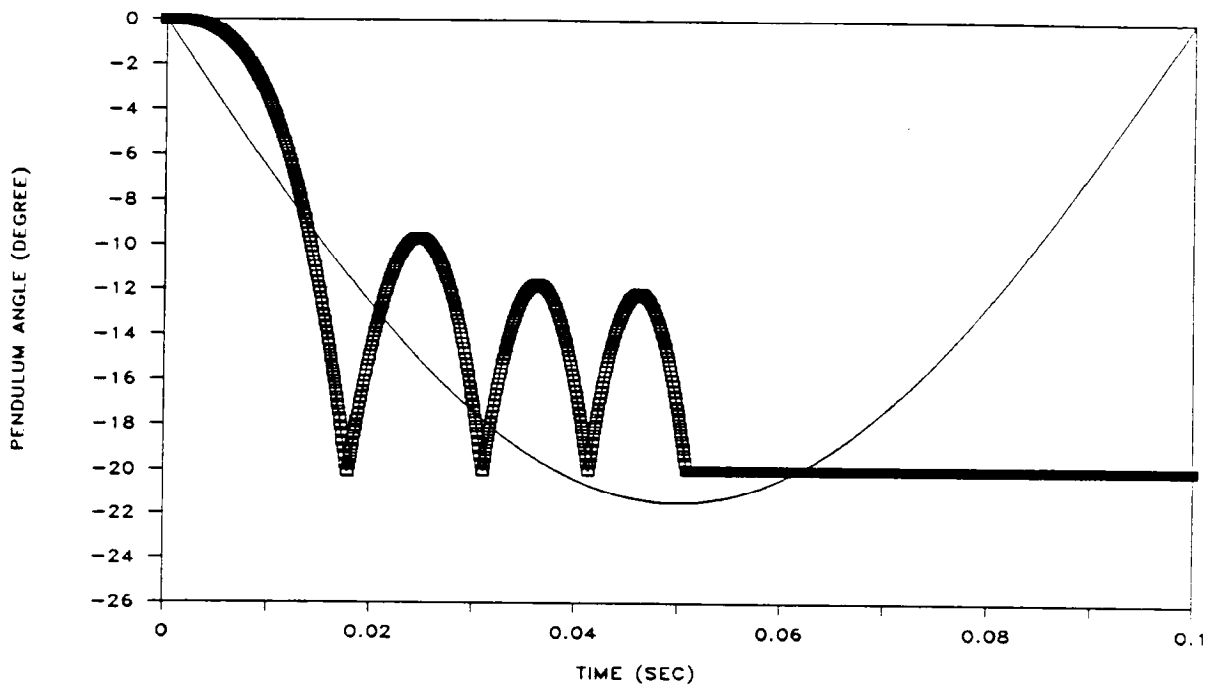


Figure 3.06 Motion of pendulum (symbols) for half sine pulse (line, in g) of $\Delta v = 48$ kph [30 mph] when $b = 2$

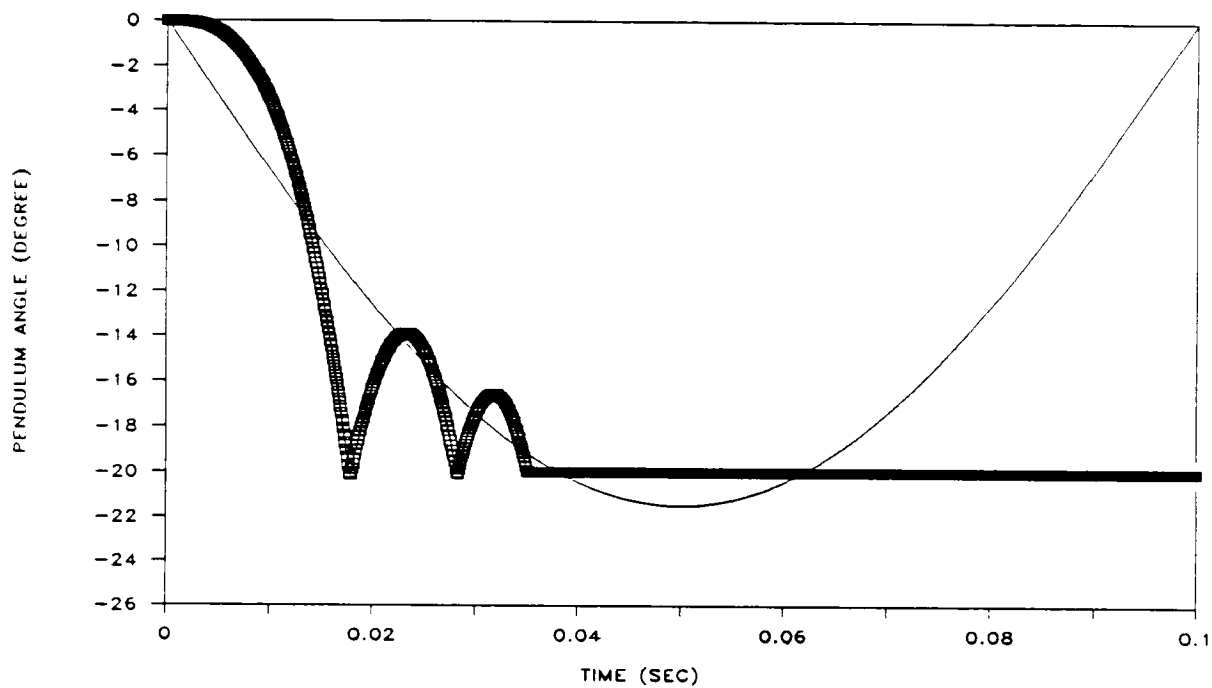


Figure 3.07 Motion of pendulum (symbols) for half sine pulse (line, in g) of $\Delta v = 48$ kph [30 mph] when $b = 5$

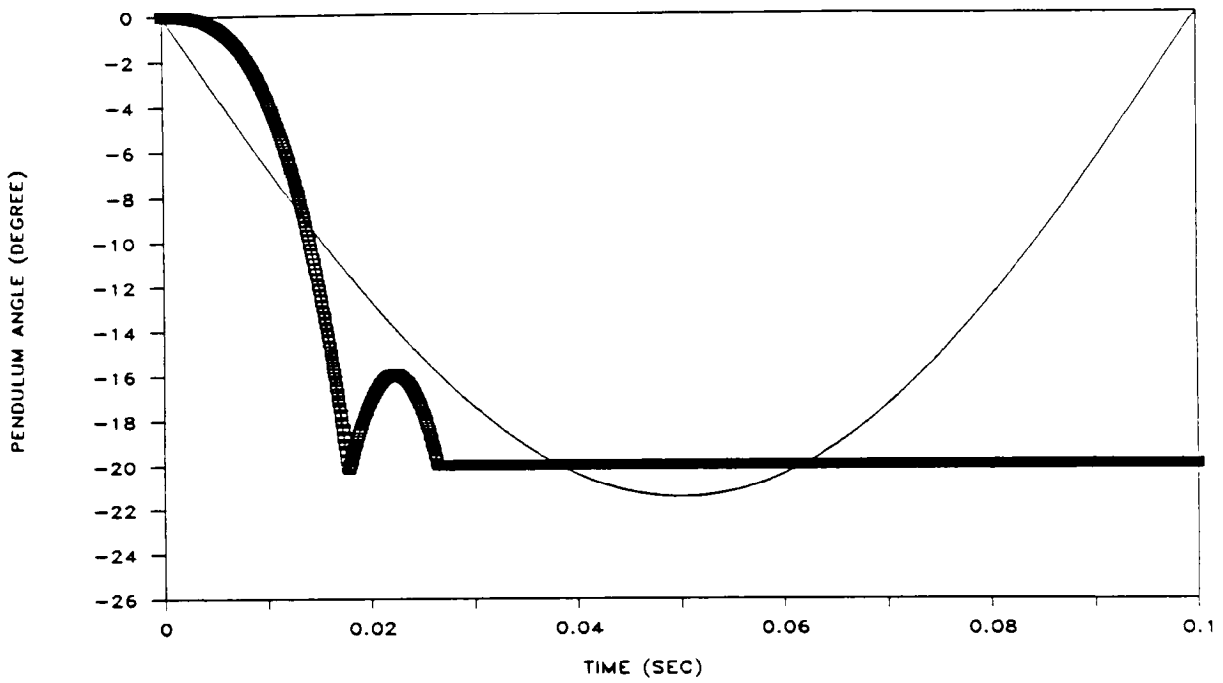


Figure 3.08 Motion of pendulum (symbols) for half sine pulse (line, in g) of $\Delta v = 48$ kph [30 mph] when $b = 7$

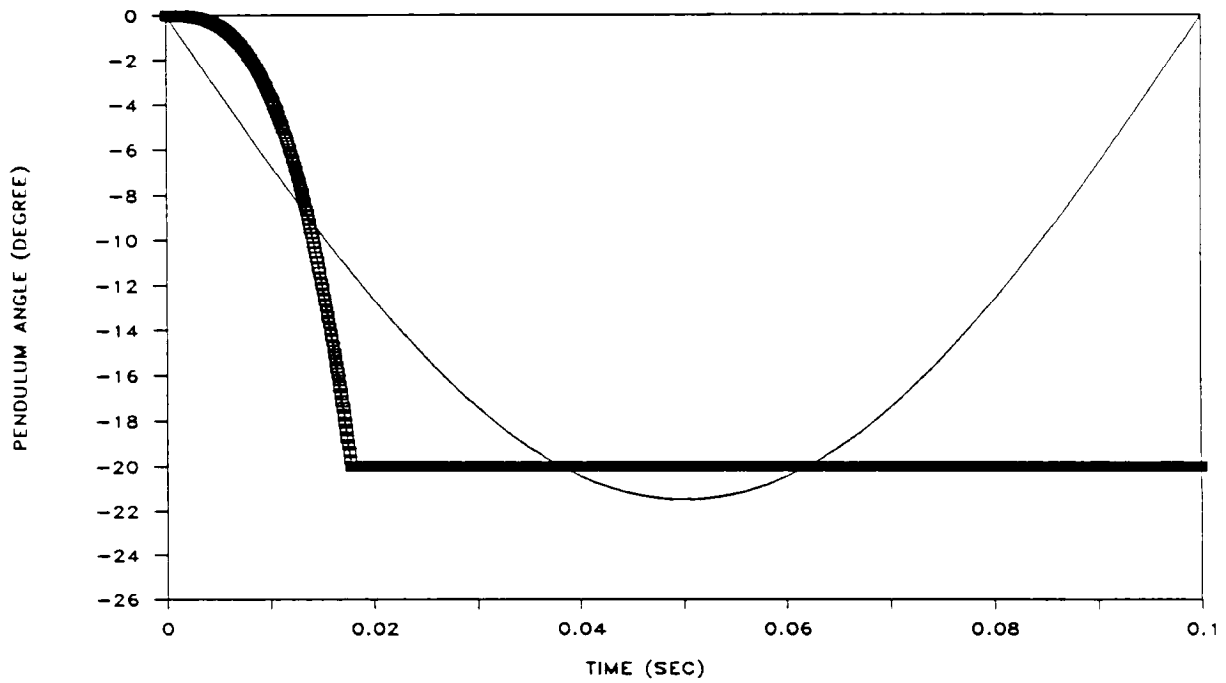


Figure 3.09 Motion of pendulum (symbols) for half sine pulse (line, in g) of $\Delta v = 48$ kph [30 mph] when $b = 10$

Table 3.1

Approximate values of b required for complete absorption
when $\Delta v = 48$ kph [30 mph] and $\Delta t = 100$ msec

Absorption coefficient b	Number of strikes n_s
~ 1	5
~ 2	4
~ 5	3
~ 7	2
~ 10	1

Table 3.2

Times (in milliseconds) to reach the first end point in
unidirectional insults with half sine wave decelerations

Change in velocity		Duration of insult (msec)			
kph	(mph)	100	120	150	200
16	(10)	26	29	34	41
32	(20)	20	23	27	32
48	(30)	18	20	23	28
64	(40)	16	18	21	26
80	(50)	15	17	20	24

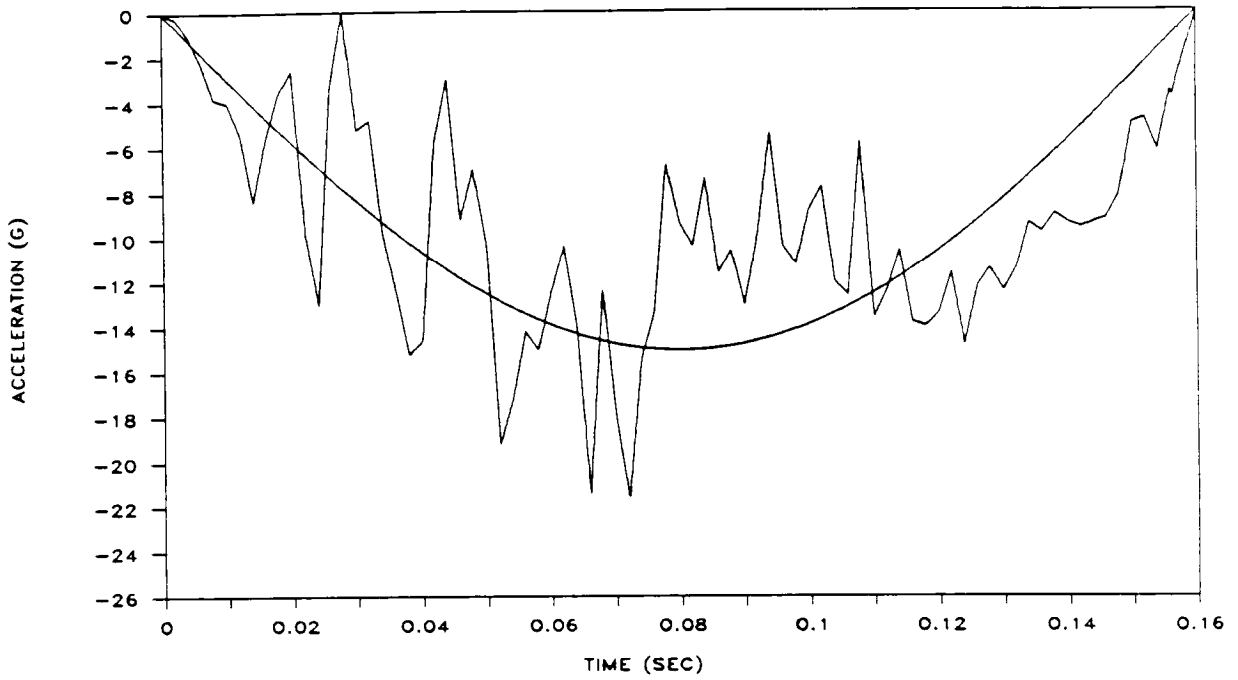


Figure 3.10 *Deceleration time histories for real-world pulse R1 (ragged line) and half sine pulse L1 (smooth line)*

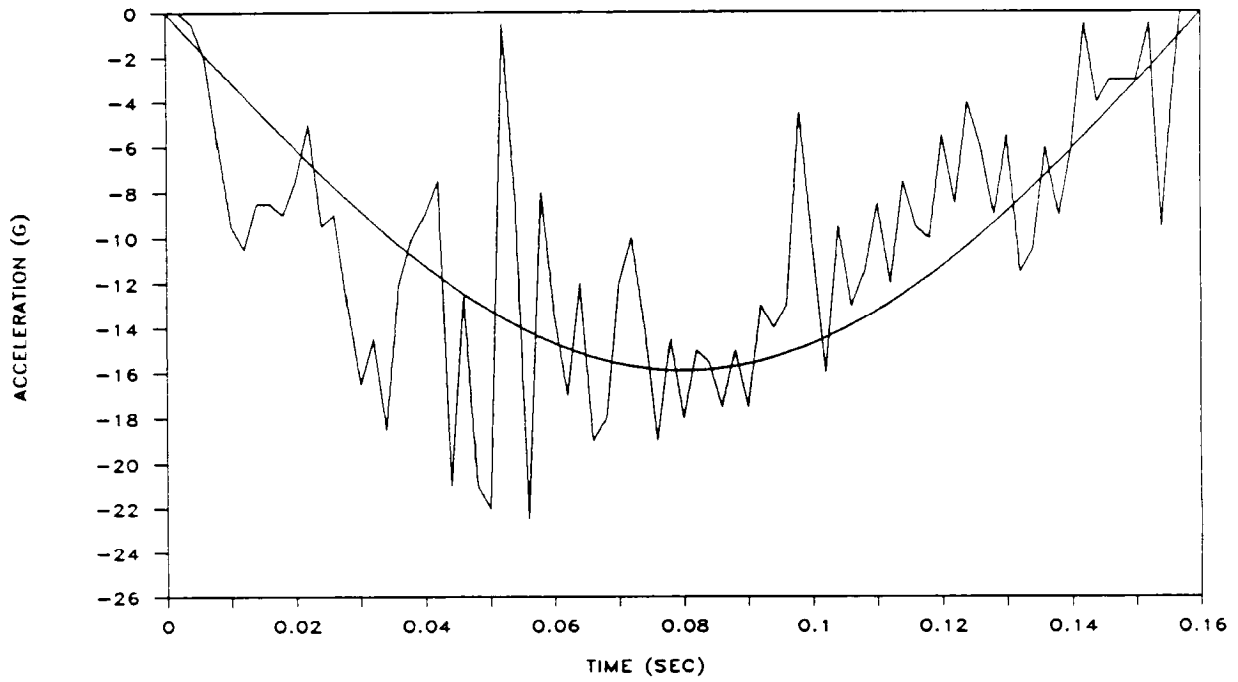


Figure 3.11 *Deceleration time histories for real-world pulse R2 (ragged line) and half sine pulse L2 (smooth line)*

time t_s , the number of strikes n_E during the impact event and the height of the local maxima even though both pulses have the same Δv and Δt . The greater maxima for the real-world pulse in Figure 3.12 represent more pronounced rebounds than for the laboratory equivalent in Figure 3.13, and they occur at greater intervals. If the activation of the safety system by the pendulum trigger is not successful at the first contact, then these greater rebounds and greater durations between rebounds in the real-world pulse may be significant.

Similar discrepancies arise in R2 and L2, as displayed in Figures 3.14 and 3.15. Again, the real-world pulse in Figure 3.14 has greater rebounds and greater durations between rebounds than the laboratory equivalent in Figure 3.15, but this would not be significant if the sensor is activated by the first contact from the pendulum trigger. A small value of b , namely $b = 0.01$, is chosen in Figures 3.12 to 3.15 to give a large enough n_E to detect any differences more readily; larger values of b will tend to reduce n_E (as seen in Table 3.1) and will therefore reduce the basis of comparison between real-world and laboratory pulses. Values from these figures are summarized in Table 3.4 for each of the four pulses.

4. Inertial sensors in multidirectional insults

4.1 General formulation

The approach described in the preceding sections for the response of a pendulum, whose pivot is driven in a single direction, may also be invoked when the pivot is simultaneously excited in more than one direction. The most obvious example of such an excitation is the bodily rotation of an inertial sensor when it is subjected to a rollover event, which is here taken to occur in the yz plane (Figure 4.01). The treatment for the motion depicted in Figure 4.01 parallels that for Figure 3.02 and yields the following counterparts to equations (3.01) to (3.06)

$$T \sin(\theta+\phi) = m y''_p \quad (4.01)$$

$$T - mg \cos(\theta+\phi) = 0 \quad (4.02)$$

$$y''_p = g \sin(\theta+\phi) \cos(\theta+\phi) \quad (4.03)$$

$$\sin(\theta+\phi) = (Y_0 - Y_p) / \ell = f_1(Y_0, Y_p) \quad (4.04)$$

Table 3.3

*Properties of some real-world unidirectional insults
and their corresponding laboratory equivalents*

		R1	L1	R2	L2
Δv	kph	54.1	54.1	57.1	57.1
	(mph)	(33.6)	(33.6)	(35.5)	(35.5)
Δt	msec	160	160	160	160
a_{MAX}	g	21.6	15.0	22.5	15.9
$v_{t=0}$	kph	51.3	54.1	71.0	57.1
	(mph)	(31.9)	(33.6)	(44.1)	(35.5)

Table 3.4

*Responses to some real-world unidirectional insults
and their corresponding laboratory equivalents*

		R1	L1	R2	L2
t_s	msec	21	23	19	23
n_E		7	8	7	9

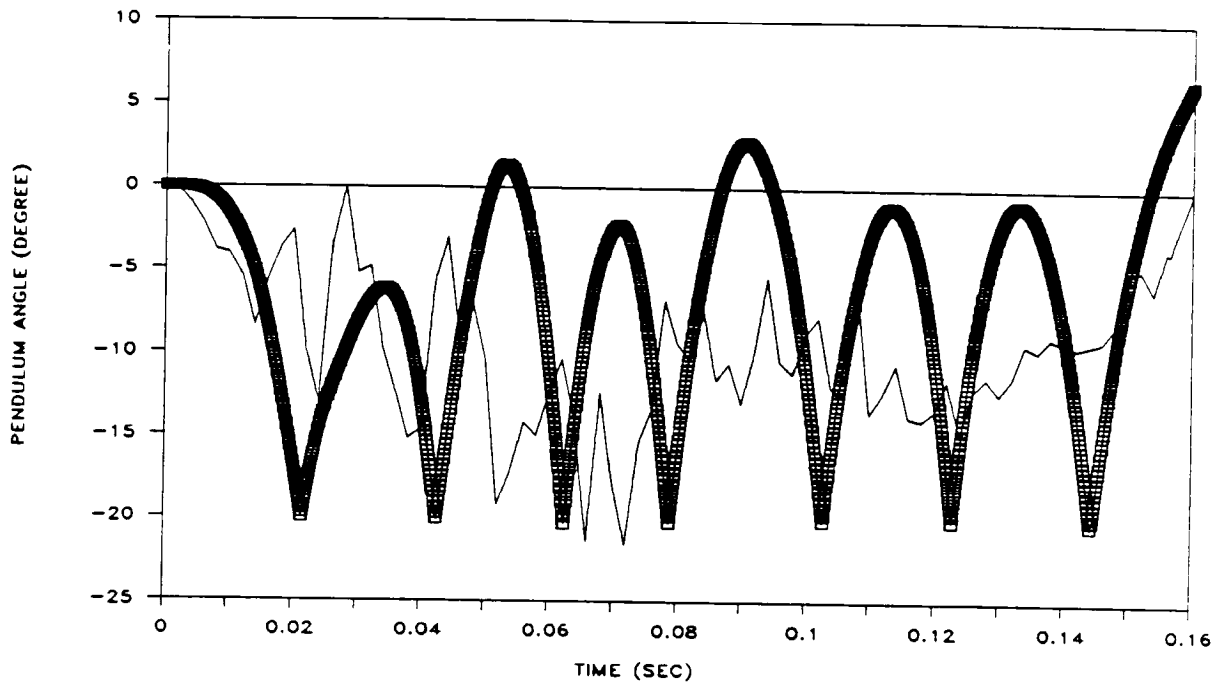


Figure 3.12 Motion of pendulum (symbols) for real-world pulse R1 (line, in g) of $\Delta v = 54.1$ kph [33.6 mph]

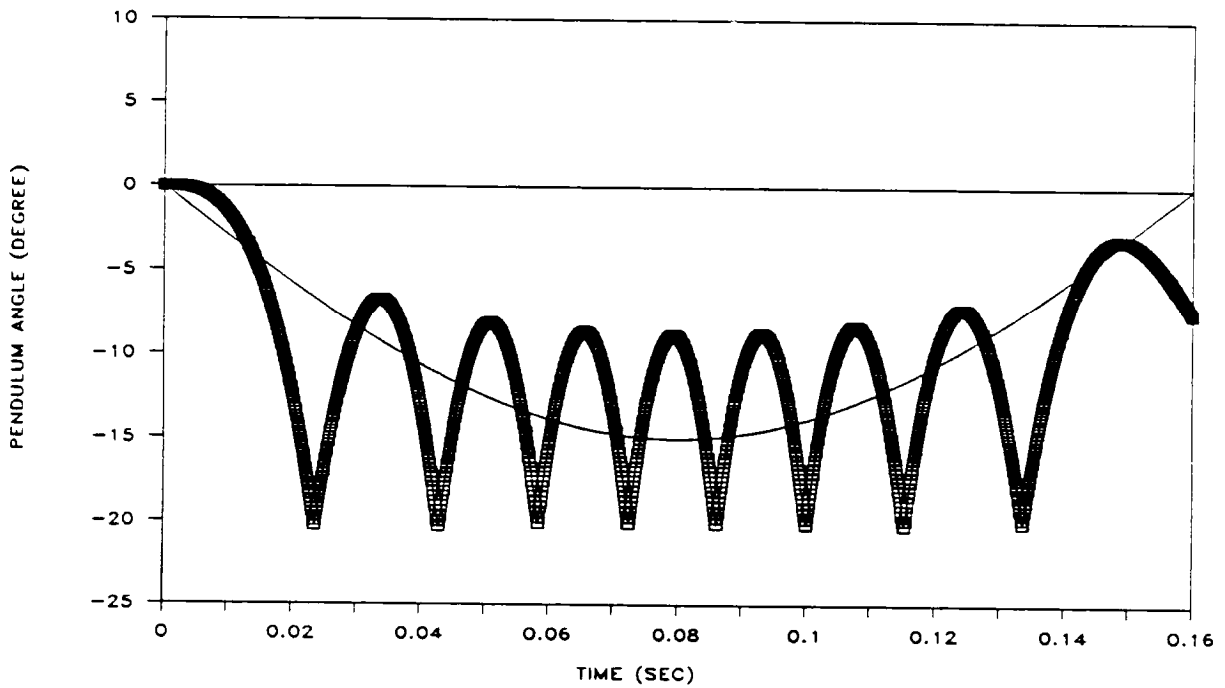


Figure 3.13 Motion of pendulum (symbols) for half sine pulse L1 (line, in g) of $\Delta v = 54.1$ kph [33.6 mph]

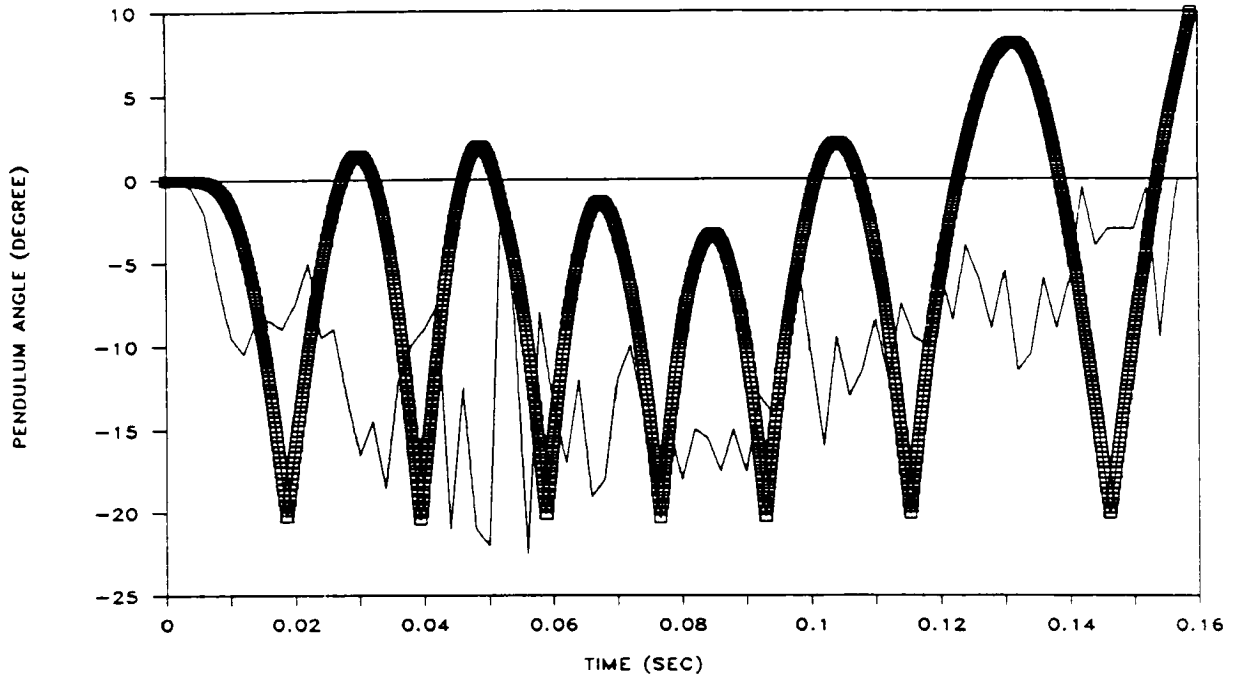


Figure 3.14 Motion of pendulum (symbols) for real-world pulse R2 (line, in g) of $\Delta v = 57.1$ kph [35.5 mph]

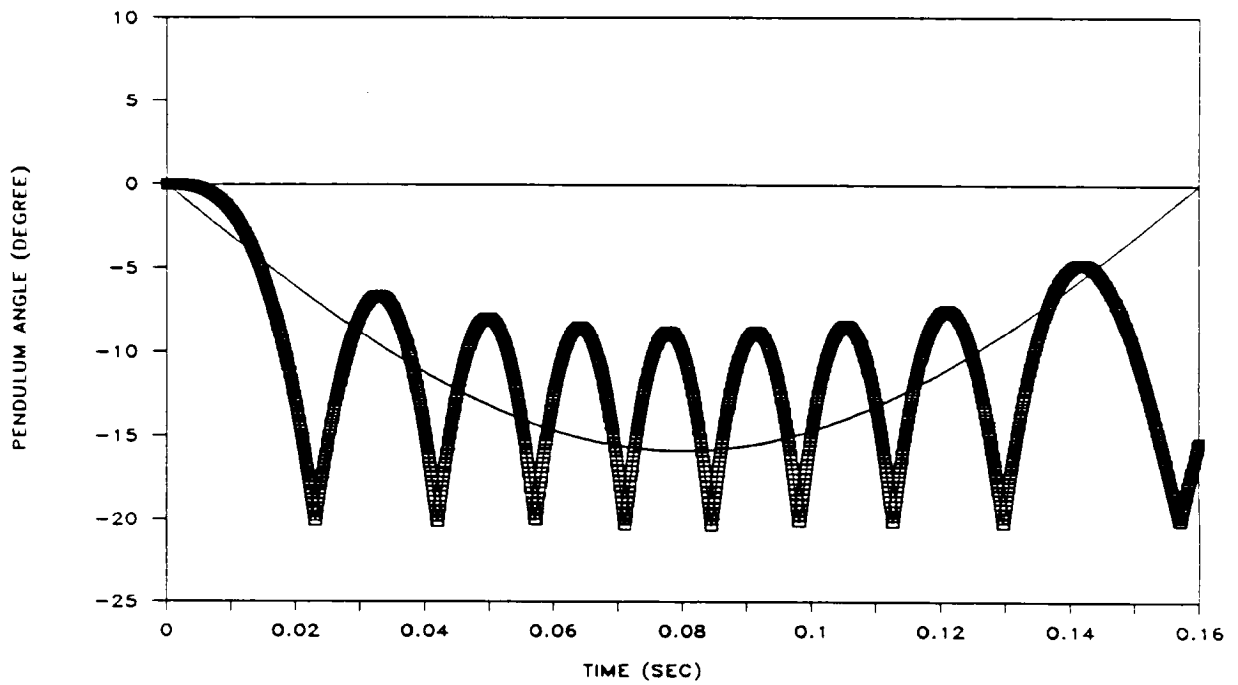


Figure 3.15 Motion of pendulum (symbols) for half sine pulse L2 (line, in g) of $\Delta v = 57.1$ kph [35.5 mph]

$$\cos(\theta+\phi) = \sqrt{1 - \sin^2(\theta+\phi)} = f_2(y_0, y_p) \quad (4.05)$$

$$y''_p = g f_1 f_2(y_0, y_p) \quad (4.06)$$

The angle ϕ is the angle between the line OC and the horizontal (where C is the center of rotation of the inertial sensor), and, for the sake of simplicity, ϕ is also taken to be the inclination of the vehicle to the horizontal. Strictly speaking, the equating of these two angles is exact only when C lies in the same horizontal plane as O at time $t = 0$, and different relationships between the two angles would need to be obtained when other geometries are present. For the simple arrangement defined here, the angle θ is the angle between the rod OP and the line perpendicular to OC.

As with equation (3.06), explicit solutions for y_p in equation (4.06) exist only for certain special y_0 . The latter may be viewed in the light of the fact that the motion of O involves a centripetal force toward the center of rotation C (Figure 4.01) so that

$$y''_o = r \phi'^2 \cos\phi \quad (4.07)$$

where r is the distance OC and ϕ' is the rate of rotation or the rollover rate. (The notation ϕ' is adopted here in preference to the alternative notation ω , which can also refer to a rate of rotation, because it provides a more obvious connection with the angle ϕ .) Actual measurements for r and ϕ' will depend on a number of factors, such as the nature of the tripping event causing the initial vehicle rotation, the location of the vehicle center of gravity, and various geometrical constraints. Particular influences on the tripping event may include the magnitude and direction of the pre-trip velocity of the vehicle, the point of contact Q where the vehicle rotation is initiated, and the viscoelastic properties of the vehicle suspension. It should be noted that C may be coincident with Q at the onset of tripping.

The pendulum is located in a seat belt retractor housing, which is usually near the side of the passenger compartment (for the upper anchor point of the shoulder belt and/or the lap belt anchor point) or near the center (for the common anchor point of the shoulder and lap belts). The following analysis uses the former as a datum for O, but the latter is also included because it is effectively among the various geometrical configurations for the former. When Q is on the same side of the vehicle as the initial location of O, the initial value of r will be small. Conversely, the initial value of r will be comparable with the width w of the passenger compartment when Q is on the opposite side of the vehicle to the initial location of O.

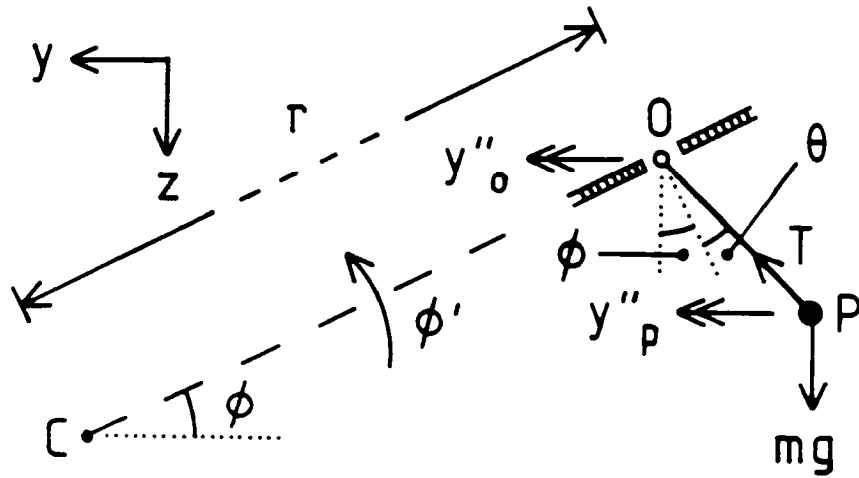


Figure 4.01 Pendulum acceleration y''_p , when smooth pivot at O is rotated about center of rotation at C

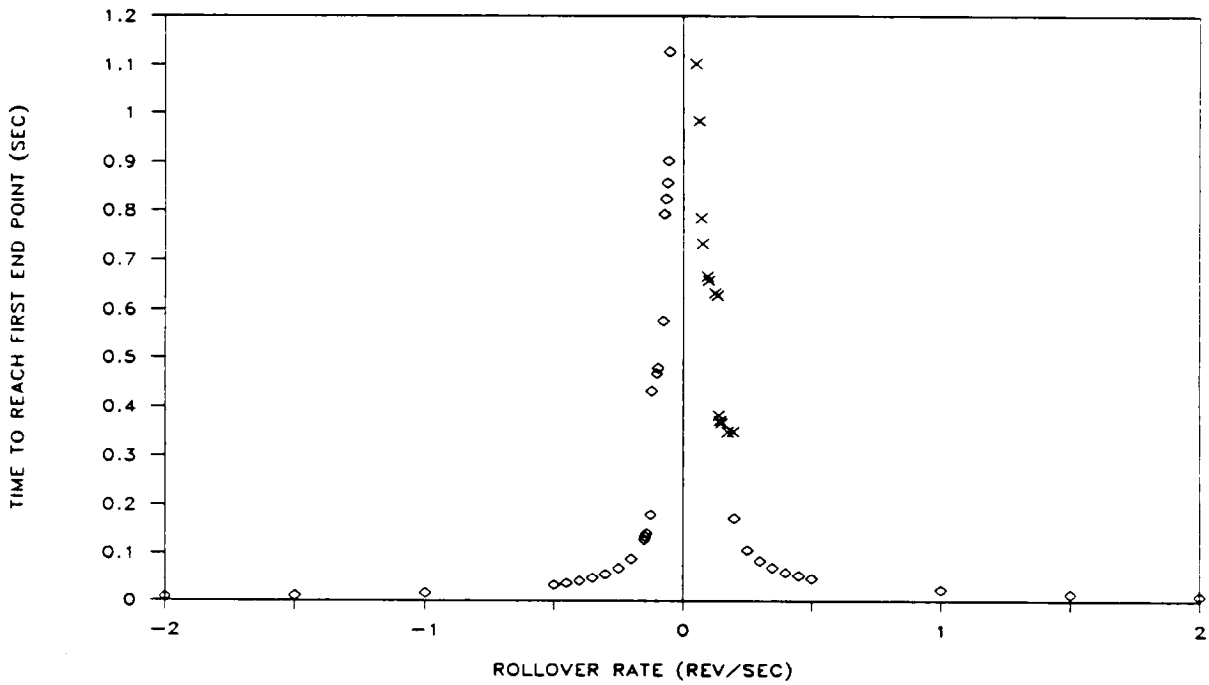


Figure 4.02 Travel time to reach first end point at $+\theta_s$ (\diamond) or at $-\theta_s$ (\times) in multidirectional insults ($r = 80$ cm)

The initial vehicle rotation about Q may be transferred into a rotation about the vehicle center of gravity G after the vehicle has left the ground. In this case, C may be associated with G and r may tend to a value of w/2 because the vehicle weight is symmetrical, or very nearly so, in the y direction. Typical values of ϕ' for this type of motion are of the order of

$$\phi' = (\pm) 1 \text{ revolution per second} \quad (4.08)$$

The rebound of the pendulum from the end points $\theta = \pm \theta_s$ (Figure 3.03) now produces a change in y'_p in the same way that x'_p was affected in equation (3.20)

$$y'_p = y'_o + c (y'_p - y'_o) \quad (4.09)$$

where c is defined in equations (3.21) to (3.25), the last of which now becomes

$$c = f_5(Y_o, Y_p) \quad (4.10)$$

Equations (4.09) and (4.10) can be combined to give

$$y'_p = f_6(Y_o, Y_p) \quad (4.11)$$

and the pendulum response governed by equations (4.06) and (4.11) may be calculated numerically.

4.2 Variation in arrival modes

The striking of one of the end points $\theta = \pm \theta_s$ by the pendulum is the first step in the activation of the inertial sensor incorporating the pendulum. It is important to realize that this step may not always be effected by the direct travel of the pendulum to one of the end points because $+\theta_s$ may be reached only after θ has been negative, or vice versa. Indeed, the pendulum may undergo multiple oscillations before one of the end points is struck. The number of oscillations n may be thought of in one of two equivalent ways: (a) as the number of local minima and maxima in θ , plus one for the actual contact with the end point; and, (b) as twice the number of points of inflexion in θ when there are no well-defined local minima or maxima, plus one for the actual contact with the end point. Different values of n distinguish the many various modes by which the pendulum reaches an end point.

These arrival modes are identified by the labels "nP" and "nN" for the two end points $+\theta_s$ and $-\theta_s$, respectively.

A typical value of r , close to half the interior width of the passenger compartment in a subcompact vehicle, may be

$$\begin{aligned} r &= 80 \text{ centimeters (cm)} \quad [\text{say}] \quad (4.12) \\ &[= 32 \text{ inches (in)}] \end{aligned}$$

For this constant value of the roll radius of the pendulum, t_s will depend on the rollover rate ϕ' and also on the arrival mode, as the results given in Table 4.1 show. One illustration of this latter dependence is the transition from arrival mode 1P to arrival mode 3P, where a one-half reduction in rollover rate produces more than a five-fold increase in arrival time. The sharp discontinuities between each arrival mode are illustrated in Figure 4.02, and the boundaries of ϕ' for each arrival mode are summarized in Table 4.2. The travel time is nearly inversely proportional to rollover rate at larger absolute values of ϕ' , corresponding to the two arrival modes 1P and 2P.

The separate arrival modes in Tables 4.1 and 4.2 can be grouped into three general categories: (a) all negative ϕ' , (b) small positive ϕ' , and (c) large positive ϕ' . An explanation for the occurrence of these broader categories of ϕ' is outlined briefly here. The gravitational and centripetal forces tend to work together when ϕ' is negative, whereas they tend to oppose when ϕ' is positive. Thus, for the same magnitude of ϕ' , a negative rollover gives a shorter time of travel to an end point than a positive rollover, as seen in the asymmetry about ϕ' in Figure 4.02. The gravitational force is greater than the competing centripetal force at low positive ϕ' but it is lower at high positive ϕ' . There is an intermediate positive ϕ' at which these forces may be matched, and the travel time becomes extremely large because arrival can be at either end point after a large number of oscillations. The exact value of this positive ϕ' cannot be identified because it lies in the discontinuous region between 2N and 2P, i.e. $+0.195 \text{ rev/sec} < \phi' < +0.200 \text{ rev/sec}$ (Table 4.2), which is shown in Figure 4.02 by the marked \diamond/\times changeover.

4.3 Combination of rollover rate and roll radius

The results in the previous section for the single rollover radius in equation (4.12) may be extended to other values of r , as summarized in Table 4.3. The general nature of the travel times in the table is outlined here briefly. An increase in r in equation (4.07) increases the centripetal force that promotes an "nP"

Table 4.1

*Travel times and arrival modes in multidirectional insults
as a function of rollover rate when $r = 80$ cm [32 in]*

Rollover rate (rev/sec)	Travel time (msec)	End point $\pm \theta_s$	Number of oscillations n	Mode
- 2.0	8	+ θ_s	1	1P
- 1.0	16	+ θ_s	1	1P
- 0.5	33	+ θ_s	1	1P
- 0.4	42	+ θ_s	1	1P
- 0.3	56	+ θ_s	1	1P
- 0.2	88	+ θ_s	1	1P
- 0.1	468	+ θ_s	3	3P
+ 0.1	660	- θ_s	5	5N
+ 0.2	173	+ θ_s	2	2P
+ 0.3	84	+ θ_s	2	2P
+ 0.4	60	+ θ_s	2	2P
+ 0.5	47	+ θ_s	2	2P
+ 1.0	23	+ θ_s	2	2P
+ 2.0	11	+ θ_s	2	2P

Table 4.2

Range of rollover rates (rev/sec) for most common arrival modes when $r = 80$ cm [32 in]

Arrival mode	Lower limit	Upper limit
1P	< - 2.000	- 0.125
3P	- 0.120	- 0.075
5P	- 0.070	- 0.055
7P	- 0.050	(< 0)
7N	(> 0)	+ 0.065
5N	+ 0.070	+ 0.135
3N	+ 0.140	+ 0.195
2P	+ 0.200	> + 2.000

Table 4.3

Times (in milliseconds) to reach the first end point in multidirectional insults

Roll radius of pendulum cm (in)	Rollover rate (rev/sec)					
	- 1.0	- 0.3	- 0.1	+ 0.1	+ 0.3	+ 1.0
5 (2)	41	150	543	569	221	202
10 (4)	35	126	532	581	246	95
20 (8)	28	100	514	603	275	55
40 (16)	22	76	490	631	328	35
80 (32)	16	56	468	660	84	23
160 (64)	12	41	157	689	53	16

arrival mode at $+\theta_s$, and this, in turn, produces a shorter travel time to $+\theta_s$. This behavior for "nP" arrival modes is inverted for "nN" arrival modes, which are shown by the shaded area in the table. While it is still true that an increase in r will increase the centripetal force, the latter now acts by decreasing the difference between it and the force due to gravity. Therefore, the net force is decreased and the travel time to $-\theta_s$ is increased.

5. Discussion

Under most typical circumstances, the inertial sensor in seat belt retractors has travel times of the order of 40 msec [say] or less in both unidirectional insults (Table 3.2) and multidirectional insults (Table 4.3), values that are similar to those for inertial sensors in supplemental restraint systems. If the pendulum strikes the end point at this time with sufficient force and duration, then the safety system will be activated and the occupant restraint system will work as intended within an acceptable timeframe. In other words, the inertial sensor will have performed its task.

There are three general sets of circumstances under which these best case scenario values of t_s may be increased dramatically:

- (1) An unsatisfactory contact with the end point by the inertial sensor could delay activation of the safety system until a second, or even later, contact. This applies to both unidirectional and multidirectional insults. (Specific aspects of the end point contact and rebound event, if any, have already been described as being beyond the scope of this research and so this difficulty is not discussed further.)
- (2) Low rollover rates of less than 0.1 rev/sec [say] can give travel times of about 500 msec (Table 4.3) for both positive and negative rollovers. Even at the higher rollover rate of 0.3 rev/sec, travel times of over 300 msec can occur.
- (3) For any given rollover radius, there is some rollover rate corresponding to the transition from the 3N arrival mode to the 2P arrival mode. This transition may be described by the region in Table 4.3 that lies between the shaded area and the non-shaded area to its right. Travel times in this region can be even higher than the extreme value of 700 msec in the table.

The delays in (2) and (3) may be serious if there is significant displacement of the vehicle occupant before the safety system is activated by the inertial sensor. The increase in travel time before the restraint system works fully can be effectively modeled by an increase in the slack in the restraint system. The latter

may be readily included as a parameter in the microcomputer version^[6-7] of the Crash Victim Simulation^[8-17] of occupant kinematics for various multidirectional insults. Preliminary results from such simulations show increasing excursions of the occupant with increasing delays in activation. The motion of the head and upper body toward the side of the vehicle is a particularly important component in these excursions, which do not occur to the same extent when the activation of the safety system is not delayed. The subsequent trauma suffered by the vehicle occupant may then be attributed, in part or in whole, to a failure of the safety system.

6. Conclusions

The three-point seat belt in passenger vehicles is a safety system that has saved untold numbers of vehicle occupants from serious injury or death. The role of the sensor that triggers this safety system is so crucial to its performance that two independent types of sensor are usually present -- one that is vehicle sensitive and one that is webbing sensitive. The performance of the former becomes critical when the response of the latter is compromised by so-called "comfort" features, e.g. windowshades, guide loops and comfort clips.

A pendulum device is one example of a vehicle sensitive sensor and its response is calculated for a variety of unidirectional and multidirectional insults. The approach adopted in this research includes some simplifying assumptions and first-order approximations, which are justified by the reasonable results obtained. The latter show that the number of occasions when the pendulum fails as an inertial sensor appears to be low. When such a failure does occur, the safety system can only provide protection if the other (webbing sensitive) sensor works properly. Therefore, both sensors must be present, and allowed to function as designed, if occasional failures of the inertial sensor are not to be catastrophic. In other words, safety systems with inertial sensors must be supplemented by the full availability of a webbing sensitive sensor. Any practice that detracts from the latter constitutes an unwarranted risk.

Acknowledgments

It is a pleasure for the author to record his appreciation and gratitude to Ed Mulligan of Edge Associates, Silver Spring, Maryland, for his support and encouragement of this study.

"Thou art worthy, O Lord, to receive glory and honour and power: for thou hast created all things, and for thy pleasure they are and were created."^[18]

References

1. Bohlin, N.I., "Säkerhetssele vid fordon," Sverige Patent 227 568, AB Volvo, Göteborg, Patenttid Från Den 29 Augusti 1958.
2. Bohlin, N.I., "Safety belt," United States Patent 3,043,625, assignor to Aktiebolaget Volvo, Göteborg, Sweden, serial number 834,258 filed August 17, 1959.
3. Bohlin, N.I., "Safety belt for vehicles," German Patent 1101987, August 24, 1959.
4. Bohlin, N.I., "Refinements of restraint system design -- a primary contribution to seat belt effectiveness in Sweden," Proceedings of International Symposium on Occupant Restraint, Toronto, Canada, June 1-3, 1981, American Association for Automotive Medicine, Morton Grove, IL.
5. Castelli, V., and Breed, D.S., "Trends in sensing side impacts," SAE Technical Paper 890603, International Congress and Exposition, Detroit, MI, February 27 - March 3, Society of Automotive Engineers, Warrendale, PA.
6. Shaibani, S.J., "The SJSATBPC package: mainframe-quality results with the Crash Victim Simulation in the microcomputer environment." Seventeenth International Workshop on Human Subjects for Biomechanical Research, Washington, DC, October 4, 1989, U.S. Department of Transportation, Washington, DC.
7. Shaibani, S.J., "The development of the SJSATBPC microcomputer package to obtain mainframe-accuracy with the Crash Victim Simulation analysis of occupant kinematics." Paper presented at 42nd Annual Meeting of American Academy of Forensic Sciences, Cincinnati, OH, February 19-24, 1990.
8. McHenry, R.R., and Naab, K.N., "Computer simulation of the automobile crash victim - A validation study." Report YB-2126-V-1R, Calspan Corporation, Buffalo, NY, July 1966.
9. Segal, D.J., and McHenry, R.R., "Computer simulation of the automobile crash victim - Revision No. 1." Report VJ-2492-V-1, Calspan Corporation, Buffalo, NY, March 1968.
10. Kidd, E.A., "Development of physical and analytical simulating of the automobile crash victim." Report VJ-2554-V-1, Calspan Corporation, Buffalo, NY, December 1970.
11. Bartz, J.A., "A three dimensional computer simulation of a motor vehicle crash victim." Report VJ-2978-V-1, Calspan Corporation, Buffalo, NY, July 1971.

12. Fleck, J.T., Butler, F.E., and Vogel, S.L., "An improved three-dimensional computer simulation of motor vehicle crash victims." Report ZQ-5180-L-1, Calspan Corporation, Buffalo, NY, 1974.
13. Fleck, J.T., Butler, F.E., and Vogel, S.L., "An improved three-dimensional computer simulation of crash victims - Volume 1: Engineering manual." Publication DOT HS 801 507, U.S. Department of Transportation, Washington, DC, April 1975. (Available through NTIS, Springfield, VA 22161, via Accession No. PB-241 692.)
14. Fleck, J.T., Butler, F.E., and Vogel, S.L., "An improved three-dimensional computer simulation of crash victims - Volume 2: Model validation." Publication DOT HS 801 508, U.S. Department of Transportation, Washington, DC, April 1975. (Available through NTIS, Springfield, VA 22161, via Accession No. PB-241 693.)
15. Fleck, J.T., Butler, F.E., and Vogel, S.L., "An improved three-dimensional computer simulation of crash victims - Volume 3: User's manual." Publication DOT HS 801 509, U.S. Department of Transportation, Washington, DC, April 1975. (Available through NTIS, Springfield, VA 22161, via Accession No. PB-241 694.)
16. Fleck, J.T., Butler, F.E., and Vogel, S.L., "An improved three-dimensional computer simulation of crash victims - Volume 4: Programmer's manual." Publication DOT HS 801 510, U.S. Department of Transportation, Washington, DC, April 1975. (Available through NTIS, Springfield, VA 22161, via Accession No. PB-241 695.)
17. Fleck, J.T., and Butler, F.E., "Development of an improved computer model of the human body and extremity dynamics." Report AFAMRL-TR-75-11, Armstrong Medical Research Laboratory, Wright Patterson Air Force Base, Dayton, OH, July 1975.
18. The Holy Bible, The Revelation of Saint John the Divine, Chapter 4, verse 11, The King James Version, 1611.

DISCUSSION

PAPER: Characteristics of Safety Systems Activated by Inertial Sensors

SPEAKER: Saami Shaibani, Liberty University

QUESTION: Don Friedman, Liability Research

Have you considered an insult associated with the structural deformation to which the assembly is mounted?

ANSWER: No I haven't. I'm just assuming that I have a well-defined insult which I can measure with accelerometers or similar and then I can plug that into my calculations. I'm not assuming any deformation. I'm assuming that the vehicle generally responds in that way and I can assume that the vehicle response is going to be similar, not necessarily identical, to the inertial sensor response. I can't, I don't know of any test results where they have mounted instrumentation right in the vicinity of the retractor housing and then be able to transfer those crash pulses rather than the general one. I think the data that I looked at I found the crash impulse nearest to the retractor housing and I then assumed the behavior of the retractor housing would correspond to that.

Q: Let me suggest that many of the circumstances that I have investigated in which the restraint system failed to activate in the most optimum way were the result of deformation of the B-post to which the assembly is mounted and/or where there were indications in tests where accelerometers were mounted on the B-post as compared to accelerometers mounted at the center of mass of the vehicle that there is a substantial difference between the pulse exposed at the B-post and the pulse which is the representative acceleration of the vehicle at its center of mass.

A: First of all, these tests, the crash pulse was measured near the B-pillar. I'm not saying that because it's at the B-pillar then that's exactly what I'd expect the housing to see as well so I'm allowing for a possible discrepancy, I don't think much of one. But these results show that there may be poor activation even under ideal circumstances when the retractor housing as a whole is not compromised by being displaced. I agree with you that if it is displaced, then we've got a second problem. But I'm saying that even if it's not displaced, we still have a problem. It's a different type of problem, but it is a problem that needs to be addressed.

Q: Guy Nusholtz, Chrysler

It seems that what you're primarily concerned with is the centrifugal acceleration associated with the roll-over rate. How did you address the initiation of the vehicle rolling over, that's a fairly quick shock phenomena that's affecting that pendulum.

A: Well, I started out by saying that this was an ideal set of calculations. What I've assumed was that the lead-in time requires having my more or less constant value of ω or what I called here at ϕ -prime but it's going to be constant after a short duration. I didn't investigate what happens during that lead-in time; that would have been an extra level of complication and I recognize that if these studies continue then that does need to be addressed.

Q: So it's possible that the pendulum could actually lock-up well before you go into the roll-over rate due to the shock?

A: It is possible, yes.